Digital Object Identifier 10.1109/PEDSTC.2019.8697785

2019 10th International Power Electronics, Drive Systems and Technologies Conference (PEDSTC)

Volume Optimization in Si igbt based dual-active-bridge converters

Hamzeh Beiranvand

Esmaeel Rokrok

Marco Liserre

Suggested Citation

H. Beiranvand, E. Rokrok and M. Liserre, "Volume Optimization in Si IGBT based Dual-Active-Bridge Converters," 2019 10th International Power Electronics, Drive Systems and Technologies Conference (PEDSTC), Shiraz, Iran, 2019.

Volume Optimization in Si IGBT based Dual-Active-Bridge Converters

Hamzeh Beiranvand and Esmaeel Rokrok
Department of Electrical Engineering
Lorestan University
Khorramabad, Lorestan, Iran
beiranvand.ha@fe.lu.ac.ir, rokrok.e@lu.ac.ir

Marco Liserre
Chair of Power Electronics
Christian-Albrechts-Universität zü Kiel
Kiel, Schleswig-Holstein, Germany
ml@tf.uni-kiel.de

***Abstract* –Dual-Active-Bridge (DAB) converters are able to step up/down DC voltage in a wide range by adopting medium frequency transformer (MFT) for isolating and converting voltage level. Increase in switching frequency of Si IGBTs reduces the MFT size instead it intensifies the semiconductor switching losses which leads to increase in the heatsink size. In this paper variation of heatsink volume versus frequency is compared versus MFT. MFT and heatsink volume of a 5 kW 600 to 400 V DAB converter are optimized. Obtained results show that variation of switching frequency in range 1-10 kHz increases the size of optimal heatsink by 3 times, i.e $V_{HS,opt} \propto \sqrt{f_s\,[kHz]}$.**

Index Terms – DAB converter, Heatsink, Medium Frequency Transformer, Volume Optimization, Efficiency.

I. INTRODUCTION

Dual-Active-Bridge (DAB) are one of the key topologies for DC voltage level transformation and galvanic isolation utilizing medium frequency transformers (MFTs) [1]. DAB converters are referred to DC transformers with excellent bidirectional power control [2] and [3]. There are many applications that are benefited from these properties such as airborne wind turbines [4], offshore wind turbines [5], electric aircraft distribution systems [6], renewable generation control [7], and solid-state smart transformers [8].

Some DC-DC converter topologies can be used to convert the DC voltage level and provide electric isolation for primary and secondary. For instance, series-resonant converter (SRC) [9] and dual H bridge (DHB) converter [10] are used as isolated DC-DC converters in the literature. SRC resonant circuit needs high voltage capacitors and a large inductor. Also, variable resonant frequency makes control system complicated. DHB topology has large reactive circulation power which results in high current inside MFT windings. While, DAB converter is able to achieve soft-switching in both primary and secondary sides, resonant inductance can be included in the MFT design and low circulating reactive power are making DAB an interesting solution.

For designing a compact DAB converter, two parts play significant role: heatsink and MFT. In the case of MFT, core cross sectional area is proportional to the inverse of frequency, $A \propto 1/f_s$, implying on weight and volume reduction by increasing the frequency [11]. Cooling surface is a function of MFT volume and therefore cooling system creates a constraint on reducing the volume of the MFT. Thermal constraint for natural convection design are more observable. It means that in Si IGBT based designs where switching frequency is limited to $fs < 10$ kHz huge volume reduction is not reachable. In the other hand, in Si IGBT based converters operating in hard-switching mode, switching losses increase exponentially with frequency. High Si IGBT losses need sufficient heatsink volume to convey heat out of the semiconductor chip which needs an optimal design to save volume.

Comprehensive efficiency-volume-weight optimization of 3-level and 5-level DAB converters based on Si IGBT and SiC MOSFET is done for a 5 kW DAB converter [12]. The paper, uses the analytical heatsink thermal model presented in [13] where heatsink fin and plate in an extruded heatsink are considered for thermal resistance network calculations. This method is relatively exact. However, it is not applicable for any fin geometry available in the market. In addition, 3D analytical models [14] and finite element method are more complex but having maximum exactness. Total thermal resistance of air forced cooling systems is lower than natural convection one and higher volume reduction is possible. When adding an air forced heatsink, an extra fan is required which enhances the overall losses and degrades the efficiency. So, only natural convection heatsink is considered in this paper.

In this paper, an analytical design procedure is used to optimize the volume of heatsink and MFT in a Si IGBT based DAB converter. Natural convection is considered in the design and therefore only the semiconductor losses including conduction, switching and reverse recovery losses are influencing the design of heatsink. Other magnetic components such as MFT and inductor, and also PCB mounted control circuits such as drivers, sensors and the DSP based controller loss contributions are not considered the design of heatsink. The method is evaluated by designing a 5 kW DAB converter which convert 600 V DC to 400 V DC. In the design example IGBT module CM100DY-24T, U-shaped N87 ferrite cores, 1-10 kHz litz wires and also Aavid Permalloy heatsink extrusions are used in the design. Design results show that minimum achievable volume based on the used materials for MFT is 1.4305 dm^3 and for heatsink the minimum volume varies from 0.165 to 0.475 dm^3 versus frequency of 1-10 kHz. Efficiency at optimal designs, neglecting the inductor, capacitor and control system losses, varies from 99% at 1 kHz to 97.2470% at 10 kHz.

978-1-5386-9254-7/19/$31.00 ©2019 IEEE

II. DAB Converter Analysis

DAB converter circuit is shown in Fig. 1 and its current and voltage waveforms for switches S_1 and S_5 are shown in Fig. 2. Primary side ac current of the MFT can be stated as:

$$i_{ac1}(t)=\begin{cases}\dfrac{I_{m1}+I_{m2}}{\varphi}t-I_{m1} & 0\le t<\varphi\\ \dfrac{I_{m1}-I_{m2}}{\pi-\varphi}(t-\varphi)+I_{m2} & \varphi\le t<\pi\\ -\left[\dfrac{I_{m1}+I_{m2}}{\varphi}(t-\pi)-I_{m1}\right] & \pi\le t<\pi+\varphi\\ -\left[\dfrac{I_{m1}-I_{m2}}{\pi-\varphi}(t-\varphi-\pi)+I_{m2}\right] & \pi+\varphi\le t<2\pi\end{cases} \quad (1)$$

Where

$$I_{m1}=\frac{1}{L_{eq}f_s}\left[-\frac{a_tV_{dc2}}{4}\left(1-\frac{2\varphi}{\pi}\right)+\frac{V_{dc1}}{4}\right] \quad (2)$$

$$I_{m2}=\frac{1}{L_{eq}f_s}\left[-\frac{V_{dc1}}{4}\left(1-\frac{2\varphi}{\pi}\right)+\frac{a_tV_{dc2}}{4}\right] \quad (3)$$

Where $a_t=V_{dc1}/V_{dc2}$ and is the phase shift between primary and secondary H-Bridges of the DAB converter. Also, V_{dc1} and V_{dc2} are the primary and secondary DC voltages, respectively. Switching frequency is denoted by f_s. Power of the converter is

$$P_N=\frac{a_tV_{dc1}V_{dc2}}{2\pi f_sL_{eq}}.\varphi.\left(1-\frac{|\varphi|}{\pi}\right) \quad (4)$$

In (4), L_{eq} is the equivalent series inductance of the MFT and inductor which guarantees power flow for a given . The ac current is used for computing the MFT winding losses.

Other important parameters are root-mean-square (rms) and average value of the currents flowing inside semiconductors.

$$i_{d1,avg}=-I_{m1}.\frac{I_{m1}}{I_{m1}+I_{m2}}.\frac{\varphi}{2T_s} \quad (5)$$

$$i_{d1,rms}=\sqrt{I_{m1}^2.\frac{I_{m1}}{I_{m1}+I_{m2}}.\frac{\varphi}{3T_s}} \quad (6)$$

$$i_{g1,avg}=I_{m2}.\frac{I_{m2}}{I_{m1}+I_{m2}}.\frac{\varphi}{2T_s}+(I_{m1}+I_{m2}).\frac{\pi-\varphi}{2T_s} \quad (7)$$

$$i_{d1,rms}=\sqrt{I_{m2}^2.\frac{I_{m2}}{I_{m1}+I_{m2}}.\frac{\varphi}{3T_s}+\left(I_{m1}^2+I_{m2}^2+I_{m1}.I_{m2}\right).\frac{\pi-\varphi}{3T_s}} \quad (8)$$

Where T_s is the inverse of switching frequency. These values are required for calculating the semiconductor losses. Semiconductor major losses are conduction, turn on, turn off and reverse recovery losses. These losses can be analytically calculated from the provided data in the manufactures' datasheets as in [15].

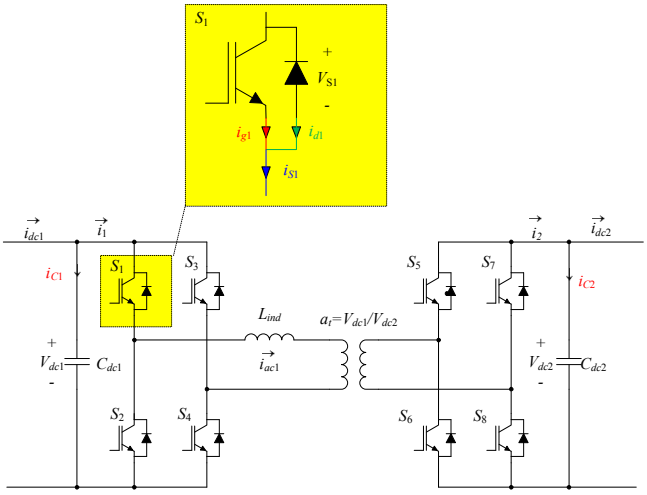

Fig. 1 DAB converter basic topology.

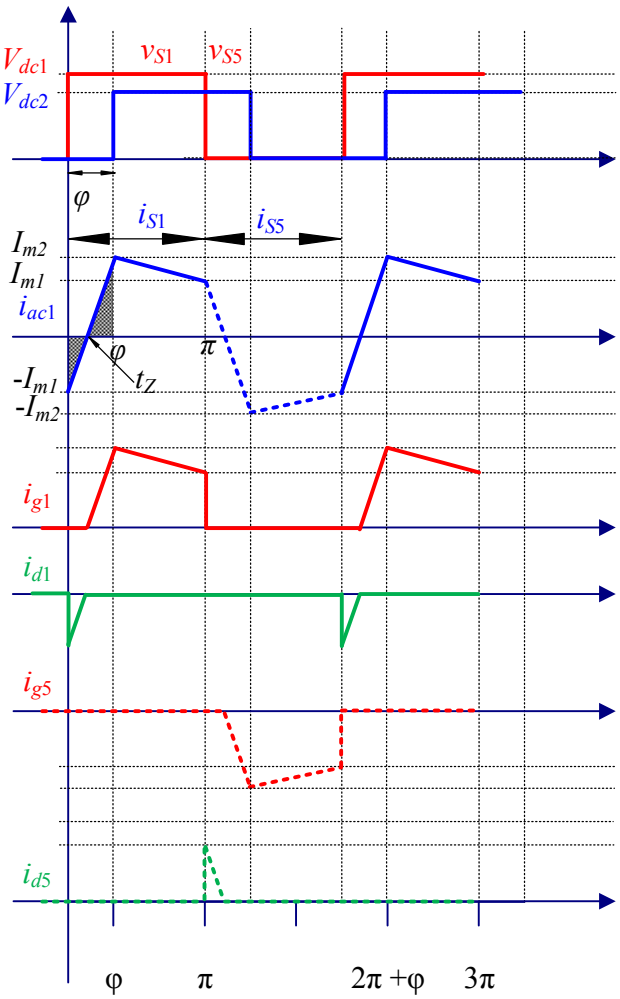

Fig. 2 DAB converter basic voltage and current waveforms required for calculating MFT and semiconductor losses. First subplot is voltage applied to the S_1 and S_5, second subplot is ac current i_{ac1}, third and fourth subplots are currents through the IGBT and diode of S_1, and fifth and sixth subplots are currents through the IGBT and diode of S_2. Note that currents of S_1 and S_2 are shown in solid and dashed lines, respectively.

III. Heatsink Design Procedure

Heatsink extrusions that are commercially available are cost effective and can be adopted for the design. First step in the heatsink design is to select the Si IGBT switches. It can be done based on the voltage and current rating of the converter. Heatsink surface temperature can be obtained by computing the IGBT power losses and using the thermal resistance of the junction to case, $R_{th,jc}$, as follows:

$$\theta_{HS} = \theta_j - R_{th,jc} P_{loss} \tag{9}$$

Maximum required thermal resistance for a heatsink to transfer the heat from heatsink surface is:

$$R_{th} \le \frac{\theta_{HS} - \theta_a}{N_{SW} P_{L,SW}} \rightarrow R_{th,\max} = \frac{\theta_{HS} - \theta_a}{N_{SW} P_{L,SW}} \tag{10}$$

Where $P_{L,SW}$ and N_{SW} are power losses per switch and number of switches, respectively. Manufacturers usually provide $R_{th,n}$ for nominal length, L_n, and temperature rise of heatsink to the ambient $\Delta\theta_n$ [16]. Correction factor curves are used to compensate $R_{th,n}$ for arbitrary L_{HS} and $\Delta\theta$ as shown in Fig. 3.

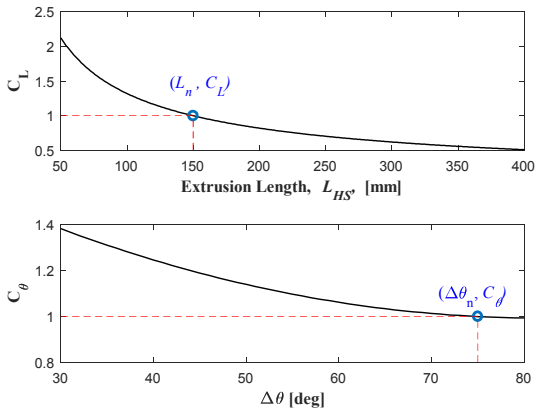

Fig. 3 Heatsink extrusion's correction factors of Aavid Permalloy LLC.

These curves can be approximated using the following equations:

$$C_L = a_L \left(L_{HS}\right)^{-b_L} \tag{11}$$

$$C_\theta = a_{\theta 0} + a_{\theta 1}\left(\Delta\theta\right) + a_{\theta 2}\left(\Delta\theta\right)^2 \tag{12}$$

Therefore, the required length correction factor and the minimum length of the extrusion can be found from the following:

$$C_L \ge \frac{R_{th,\max}}{C_\theta R_{th,n}} \tag{13}$$

$$L_{HS,\min} = \left(C_L / a_L\right)^{-\frac{1}{b_L}} \tag{14}$$

Based on the $L_{SH,min}$ total weight and volume of the extrusion are computed.

Flowchart of the heatsink design is shown in Fig. 4. Based on the figure, IGBT rating is the start point of the design. After selection of the IGBT switch ratings, its data can be used to drive the conduction, turn on and turn of losses as well reverse recovery losses. The semiconductor loss calculation method is based on the Drofenik paper given in [15]. So, after calculation of power loss per IGBT (P_{loss}) and also by using the junction to case thermal resistance ($R_{th,jc}$) the heatsink surface temperature (θ_{HS}) can be obtained. In this paper, maximum allowable junction (θ_j) and ambient temperature (θ_j) are 125 ˚C and 40 ˚C, respectively.

An optimal heatsink extrusion must be able to convey the semiconductor heat with minimum size and weight. Extrusion's cross section is usually constant and the only variable is the length for commercially available extrusion's [16]. Based on the equation (14) minimum length of extrusions for any proper extrusion model can be calculated. Extrusion's weight and volume can be directly computed from the length. In this paper, natural convection is considered. However, forced convection can be simply achieved by adopting related thermal resistance and correction factor.

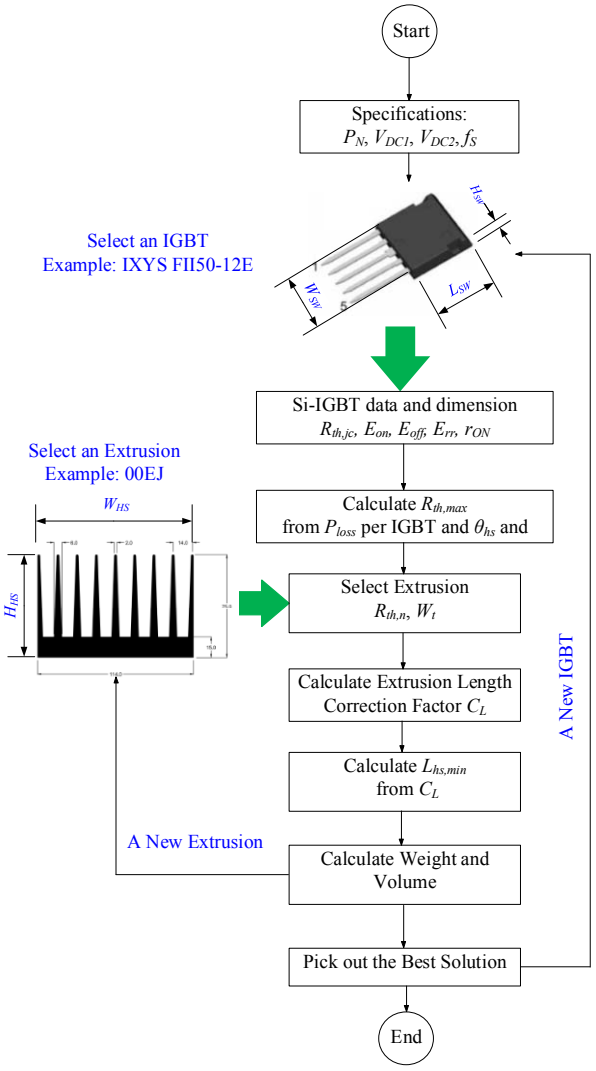

Fig. 4 Heatsink design flowchart.

IV. MFT Design Procedure

In this paper, MFT optimization is done based on the [17]. Generally, core and winding losses are the main losses in MFTs and are considered in the most of the researches. However, some papers consider the insulation material capacitive losses such as [18] and [19]. In these paper, the insulation material capacitive losses are neglected in the optimization procedure.

Fig. 5 (a) shows an half of a U-core based MFT and related dimensions that is adopted for constructing MFTs with N87 ferrite material.

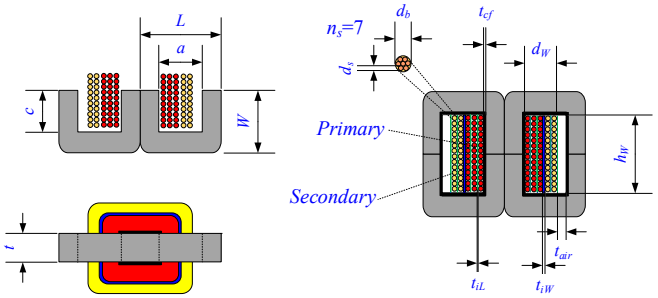

Fig. 5 MTF constructed using N87 ferrite U-cores; (a) U-core main dimensions, and (b) concentric winding dimensions.

A. Core Losses

Non-sinusoidal voltage waveform supplying the MFT yields non-sinusoidal flux density waveform in the ferrite core. Improved generalized Steinmetz equation (IGSE) can be employed to approximate N87 ferrite core losses [20]. IGSE is an updated version of generalized Steinmetz equation (GSE) which is presented in [21]. IGSE improves the deficiency of GSE in calculation of the losses due to minor hysteresis loops. IGSE includes the minor hysteresis losses by using their peak-to-peak amplitude of flux density in the same way that GSE uses peak-to-peak amplitude of flux density of major hysteresis loops to compute core losses.

A. Copper Losses

Copper losses, P_{CU}, can be calculated using the following formula:

$$P_{CU,p} = \frac{2N_p MLT_p}{\sigma_{CU}\left(\pi n_s d_s^2\right) pf} \sum_{n=1}^{N_h} F_n \left(a_n^2 + b_n^2\right) \qquad (15)$$

Where, MLT is the mean-length-turn of the winding, N_p is the number of turns in the primary side of the MFT, σ_{CU} is the conduction of copper, d_s and n_s are strands diameter and number, respectively. Dowells resistance factor, F, is adopted for calculating high frequency effects on the round litz wire resistance [22]. Also, pf is the packing factor. Packing factor and other dimensional variables can be defined based on the winding geometry given in Fig. 5 (b) as follows:

$$pf = n_s \left(\frac{d_s}{d_b}\right)^2 \qquad (16)$$

$$MLT = 2\left(a + N_{cp} t\right) + 2\pi\left(t_{cf} + \frac{d_W}{2}\right) \qquad (17)$$

$$\begin{aligned} d_W &= m_1 d_{b1} + m_2 d_{b2} + (m_1 - 1)t_{iL1} + (m_2 - 1)t_{iL2} + M t_{iW} \\ h_{Wmax} &= 2c - t_{df} \end{aligned} \qquad (18)$$

$$m_1 = \left\lceil (N_1 + 1)\frac{d_{b1}}{h_{Wmax}} \right\rceil, m_2 = \left\lceil (N_2 + 1)\frac{d_{b2}}{h_{Wmax}} \right\rceil \qquad (19)$$

Where N_1 can be calculated from Faraday's law of induction as:

$$N_1 = \frac{V_{dc1}}{4 f_s B_{mag} A_c} \qquad (20)$$

In these equations, M is the number of magnetic sections, h_{Wmax} is possible maximum winding height. Geometry and thermal constraints are:

$$h_{Wmax} \geq \max\left(d_{b1}\frac{N_1 + 1}{m_1}, d_{b2}\frac{N_2 + 1}{m_2}\right) \qquad (21)$$

$$t_{air} = \frac{b - a}{2} - 2t_{cf} - d_W \geq 0 \qquad (22)$$

$$\Delta T_m - R_{th}(P_C + P_{CU,p} + P_{CU,c}) \geq 0 \qquad (23)$$

Where R_{th} is the thermal resistance, P_C is the core losses and ΔT_m is the maximum allowable temperature rise.

A. Design Procedure

Fig. 6 shows the design and optimization method adopted in this paper.

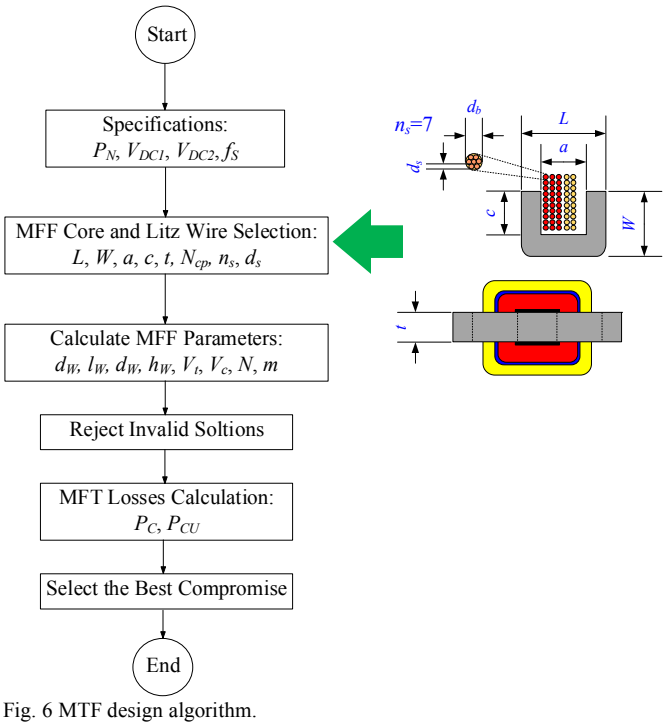

Fig. 6 MTF design algorithm.

V. Simulation Results

An example 5 kW 600 to 400 V DAB converter is considered as a design example. Semiconductor losses are computed for sizing the heatsink. Capacitors and inductor losses are neglected. In the following subsections, MFT and heatsink optimization are given.

A. MFT Optimal Design

For constructing MFT, 20 round litz wires for f_s=1-10 kHz from New-England Wire Technologies [23], six N87 ferrite U cores from Epocs AG [24] and potted EPOXY with dielectric strength of 16 kV/mm from Mouser Electronics and loss tangent of 0.02 at 100 kHz [18] are used. In addition, maximum number of parallel cores is set to N_{cp}=3 and peak of flux density is consider in range 0.2 to 0.3 Tesla in 0.01T steps. Therefore, total number of solutions is calculated from all possible solutions 10×6×20×20×3×10=720000. Acceptable solutions are depicted in Fig. 7. It is seen from the figure that efficiency of the MFT reduces by increasing the frequency. Minimum volume is 1.4305 dm^3 where power density (ρ) is 3.4954 kW/dm^3.

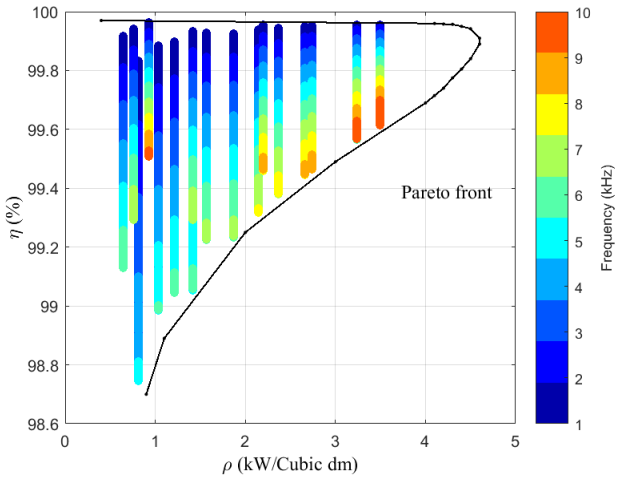

Fig. 7 Power losses versus Volume for MFT designs at 10 frequencies from 1 up to 10 kHz.

B. Heatsink Optimal Design

The start point for designing heatsink is to estimate DAB converter power losses. MFT and semiconductor losses are shown in Fig. 8 as a function of frequency. 1200 V, 100 A IGBT module CM100DY-24T of Mitsubishi Electric is considered in this example design where its loss details can be found in [25]. For heastsik, 138 extrusions are selected with flat surface for mounting Si-IGBT modules from Aavid Permally LLC [16]. Four possible configurations are considered which are shown it table I. The table also include the best heatsink solutions at different frequencies. The results are also shown in in Fig. 9 where blue and red colors show configuration 1 and 4, respectively. Volumes larger than 1 dm^3 are removed from this figure. Every solid line shows the obtained volume of a heatsink extrusion.

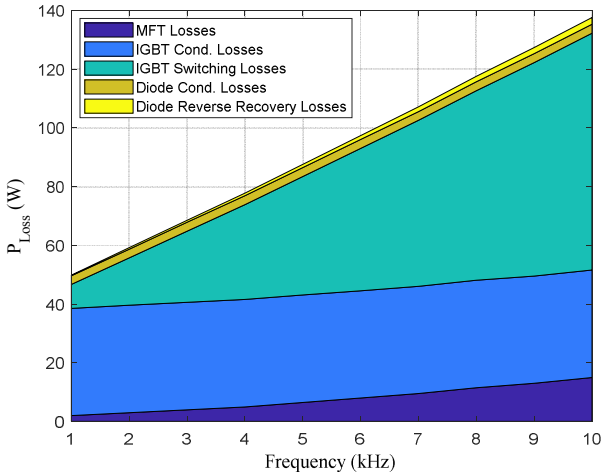

Fig. 8 Detailed power losses at 10 frequencies from 1 up to 10 kHz. At high frequencies, switching losses dominate the other losses due to hard switching.

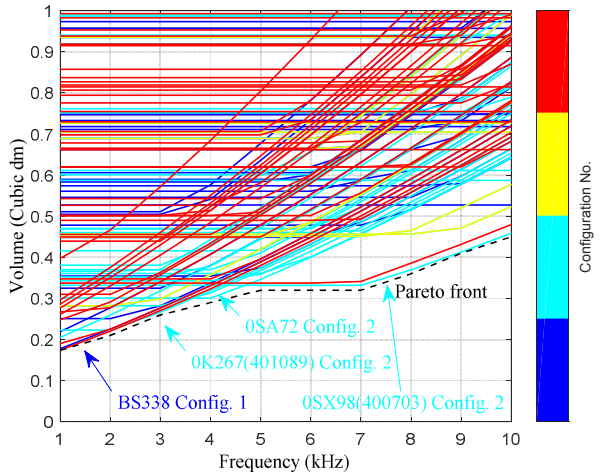

Fig. 9 Heatsink volume at 10 frequencies from 1 up to 10 kHz. At high frequencies, volume increases.

C. Overview Results

Obtained results show that heatsink volume increases from 0.165 to 0.475 when switching frequency varies from 1 to 10 kHz. It shows the size increases 3 times. While, in this frequency range, the volume of MFT doesn't change significantly. Based on the results given in table I, extrusion number BS338 is the best solution for frequencies 1 and 2 kHz. Using BS338 for other frequencies such as 10 kHz results in a volume of 0.8 dm^3 and using OSA72 gives 0.65 dm^3. The results imply on the effect of frequency on the selected heatsiks. Total volume of the IGBT modules is 0.373 dm3. This value can be further reduced by selecting more compact IGBTs such as IXYS-FII50-12E which has current rating of 100 A at 25 ˚C. Semiconductor technology directly affect the heatsink design due to the amount of the generated losses. I the next work, effect of Si IGBT, SiC MOSFET and GaN will be evaluated on the heatsink volume.

It can be concluded that for Si IGBT based DAB converters operating in hard switching mode, heatsink volume increases rapidly and can be a limiting constraint for application where volume is a priority.

TABLE I
HEATSINK PARAMETERS FOR DESIGN AND OPTIMAL RESULTS

Configurations	1	$W_{HS}>1.1\times L_{SW}$	$L_{HS}>1.1\times 4\times W_{SW}$
	2	$W_{HS}>1.1\times 4\times W_{SW}$	$L_{HS}>1.1\times L_{SW}$
	3	$W_{HS}>1.1\times 2\times L_{SW}$	$L_{HS}>1.1\times 2\times W_{SW}$
	4	$W_{HS}>1.1\times 2\times W_{SW}$	$L_{HS}>1.1\times 2\times L_{SW}$
Optimal Extrusions	1-2 kHz	BS338	Config. No. = 1
	3 Hz	0k267	Config. No. = 2
	4 Hz	0SA72	Config. No. = 2
	5-10 Hz	0SX98	Config. No. = 2
Si-IGBT	Module: CM100DY-24F, Vol.=0.373 dm^3		
MFT	Vol.= 1.4305 dm^3		
Total Vol. of MFT, IGBTs and Heatsink	1 kHz	Vol.= 1.9785 dm^3	
	5 kHz	Vol.= 2.1235 dm^3	
	10 kHz	Vol.= 2.2535 dm^3	

VI. CONCLUSION

An analytical method is employed in the paper to evaluate the optimal volume of the heatsink as well medium frequency transformer (MFT). Basic data provided by manufacturers of heatsink extrusions in the data sheets are used to compute the minimum length of the extrusions. Mounting and dimensional constraints are also considered in the design procedure. Optimization is done for an example 5 kW 600 to 400 V dual-active-bridge with two H-Bridges and an isolating MFT. Simulation results show that the volume of the optimally designed heatsinsk is proportional to the square root of frequency in kHz. So, when frequency varies from 1 to 10 kHz, heatsink optimal volume increases close to three times. While, in this case, MFT volume variation is not considerable.

REFERENCES

[1] L. Costa, G. Buticchi, and M. Liserre, "Quad-Active-Bridge DC-DC Converter as Cross-Link for Medium Voltage Modular Inverters," *IEEE Transactions on Industry Applications,* vol. PP, pp. 1-1, 2016.

[2] M. J. Carrizosa, A. Benchaib, P. Alou, and G. Damm, "DC transformer for DC/DC connection in HVDC network," in *Power Electronics and Applications (EPE), 2013 15th European Conference on*, 2013, pp. 1-10.

[3] B. Zhao, Q. Song, J. Li, Y. Wang, and W. Liu, "Modular multilevel high-frequency-link DC transformer based on dual active phase-shift principle for medium-voltage DC power distribution application," *ieee transactions on power electronics,* vol. 32, pp. 1779-1791, 2017.

[4] R. Friedemann, F. Krismer, and J. W. Kolar, "Design of a minimum weight dual active bridge converter for an airborne wind turbine system," in *Applied Power Electronics Conference and Exposition (APEC), 2012 Twenty-Seventh Annual IEEE*, 2012, pp. 509-516.

[5] P. Kjaer, Y. Chen, and C. Dincan, "DC collection: Wind power plant with medium voltage dc power collection network," in *ECPE Workshop on Smart Transformers for Traction and Future Grid Applications, Zurich, Switzerland*, 2016.

[6] G. Buticchi, L. F. Costa, and M. Liserre, "Multi-port DC/DC converter for the electrical power distribution system of the more electric aircraft," *Mathematics and Computers in Simulation,* 2018/10/01/ 2018.

[7] B. Zhao, Q. Song, W. Liu, and Y. Sun, "Overview of dual-active-bridge isolated bidirectional DC–DC converter for high-frequency-link power-conversion system," *IEEE Transactions on Power Electronics,* vol. 29, pp. 4091-4106, 2014.

[8] M. Liserre, G. Buticchi, M. Andresen, G. De Carne, L. F. Costa, and Z.-X. Zou, "The Smart Transformer: Impact on the Electric Grid and Technology Challenges," *IEEE Industrial Electronics Magazine,* vol. 10, pp. 46-58, 2016.

[9] L. F. Costa, G. Buticchi, and M. Liserre, "Highly Efficient and Reliable SiC-Based DC–DC Converter for Smart Transformer," *IEEE Transactions on Industrial Electronics,* vol. 64, pp. 8383-8392, 2017.

[10] F. Xue, R. Yu, S. Guo, W. Yu, and A. Q. Huang, "Loss analysis of GaN devices in an isolated bidirectional DC-DC converter," in *Wide Bandgap Power Devices and Applications (WiPDA), 2015 IEEE 3rd Workshop on*, 2015, pp. 201-205.

[11] M. Mogorovic and D. Dujic, "Thermal modeling and experimental verification of an air cooled medium frequency transformer," in *19th European Conference on Power Electronics and Applications (EPE'17 ECCE-Europe)*, 2017.

[12] R. M. Burkart and J. W. Kolar, "Comparative – – Pareto Optimization of Si and SiC Multilevel Dual-Active-Bridge Topologies With Wide Input Voltage Range," *IEEE Transactions on Power Electronics,* vol. 32, pp. 5258-5270, 2017.

[13] U. Drofenik, G. Laimer, and J. W. Kolar, "Theoretical converter power density limits for forced convection cooling," in *Proceedings of the International PCIM Europe 2005 Conference*, 2005, pp. 608-619.

[14] A. Castelan, B. Cougo, S. Dutour, and T. Meynard, "3D analytical modelling of plate fin heat sink on forced convection," *Mathematics and Computers in Simulation,* 2018/10/10/ 2018.

[15] U. Drofenik and J. W. Kolar, "A general scheme for calculating switching-and conduction-losses of power semiconductors in numerical circuit simulations of power electronic systems," in *Proceedings of the 2005 International Power Electronics Conference (IPEC'05), Niigata, Japan, April*, 2005, pp. 4-8.

[16] "2002 Extrusion Selection Guide Power Profiles for the European Market," ed. New Hampshire: Aavid Thermalloy, 2002.

[17] H. Beiranvand, E. Rokrok, B. Rezaeealam, and A. Kumar, "Optimal design of medium-frequency transformers for solid-state transformer applications," in *2017 8th Power Electronics, Drive Systems & Technologies Conference (PEDSTC)*, 2017, pp. 154-159.

[18] G. Ortiz, J. Biela, and J. W. Kolar, "Optimized design of medium frequency transformers with high isolation requirements," in *IECON 2010-36th Annual Conference on IEEE Industrial Electronics Society*, 2010, pp. 631-638.

[19] M. A. Bahmani, "Design and Optimization Considerations of Medium-Frequency Power Transformers in High-Power DC-DC Applications," Chalmers University of Technology, 2016.

[20] K. Venkatachalam, C. R. Sullivan, T. Abdallah, and H. Tacca, "Accurate prediction of ferrite core loss with nonsinusoidal waveforms using only Steinmetz parameters," in *IEEE Workshop on Computers in Power Electronics*, 2002, pp. 36-41.

[21] J. Li, T. Abdallah, and C. R. Sullivan, "Improved calculation of core loss with nonsinusoidal waveforms," in *Industry Applications Conference, 2001. Thirty-Sixth IAS Annual Meeting. Conference Record of the 2001 IEEE*, 2001, pp. 2203-2210.

[22] P. Dowell, "Effects of eddy currents in transformer windings," *Electrical Engineers, Proceedings of the Institution of,* vol. 113, pp. 1387-1394, 1966.

[23] "Llitz Wire Technical Information," ed: New England Wire Technologies, 2005.

[24] A. Epcos, "Ferrites and accessories," *Epcos AG Application notes,* pp. 15-17, 2006.

[25] M. Electric, "CM100DY-24T : 1200V 100 A High Power IGBT module," ed: Mitsubishi Electric, 2018.